中國機械工程學刊第三十九卷第六期第 565~574 頁(民國一百零七年)
Journal of the Chinese Society of Mechanical Engineers, Vol.39, No.6, pp 567~576 (2018)

Five-Axis Slerp for Tool-Orientation Planning in a Five-Axis CNC Machine

Chang Dau Yan *, Wei-Hua Chieng ** and Shyr-Long Jeng ***

Keywords: CNC mechanism, Planning, Slerp.

ABSTRACT

The quaternion spherical linear interpolation method (slerp), which many researchers have adopted for numerical control, is inadequate for tool-axis-orientation planning in general five-axis computer numerical control machines. This paper explains why the quaternion slerp method fails to achieve constant rotational speed. The machining quality is degraded when the quaternion slerp method is used in five-axis machining. To compensate for this failure, this paper proposes a solution for tool-axis-orientation planning, the five-axis slerp method, which generates steady angular velocity of the interpolation curve.

INTRODUCTION

Five-axis machine tools accurately machine complicated products. Two revolving axes are synchronously controlled along with three translating axes to manipulate the tool-axis orientation with respect to the piece being machined. The objective is to achieve accurate and steady movement along the tool-axis orientation to prevent low-quality products. The Euler angle method of mathematical modeling for tool-axis orientation is widely used (Henderson, 1997); however, it suffers from the gimbal-lock effect (Shoemake , 1985), (Dam et al., 1998). The quaternion method, which has favorable properties, is not only free of the gimbal-lock effect but also facilitates analytical manipulations. Thus, it has become increasingly widely employed.

Quaternion interpolation is applied to obtain a certain intermediate orientation between two specified key frames in animations. Shoemake (1998) constructed a spherical Bezier curve to interpolate several specified key orientations for animated features and calculated successive orientations in between by using recursive spherical linear interpolation (slerp) of key quaternions on different Bezier curves sliced together in the manner of splines. Barr *et al.* (1992) proposed a discrete derivative approach for interpolating orientations with quaternion curves on the unit quaternion space by minimizing the total energy function subject to angular velocity constraints. Ramamoorthi and Barr (1997) further introduced a criterion for automatic refinement based on the Euler–Lagrange error function to accelerate the construction of quaternion spline curves upon which a relatively steady interpolation can be maintained.

Ho *et al.* (2003) proposed the tool orientation smoothing (TOS) method for five-axis machining to interpolate smooth tool-axis directions from the representative tool-axis orientations in general areas to avoid interference in tool-path generation by using the computer-aided manufacturing (CAM) module. The TOS method coupled with the cutting error improvement method reduced cutting errors and increased machining efficiency by modifying the cutter location data and rearranging the tool-axis orientations. Zhang *et al.* (2014) obtained a smoother trajectory for tool-axis orientations by fitting quaternion B-spline curves and accordingly optimizing unit quaternion space. Li and Guo (2009) introduced a dual-quaternion representation of both orientation and position for five-axis machining and developed the quaternion-quintic spherical Bezier-spline-interpolation algorithm to synchronously enable five-axis orientation and positioning for superior machining efficiency and surface quality. Zhao *et al.* (2017) further selected the dominant points that can characterize the path among specified positions and orientations of five-axis machining and therefore generated a smooth tool path by using the dual-quaternion B-spline approximation method. Our proposed scheme is expected to significantly reduce the number of points for fitting and increase computational efficiency for real-time trajectory generation.

Previous studies on improving the control of tool-axis orientation have relied on the slerp method or its derivatives. Dam *et al.* (1998) analyzed the angular velocity of the interpolation curve in a unit quaternion space. The results applied to animated objects

Paper Received July, 2018. Revised October, 2018. Accepted November, 2018. Author for Correspondence: Wei-Hua Chieng

**Graduate Research Assistant, Department of Mechanical Engineering, National Chiao Tung University, Taiwan, ROC.*

***Professor, Department of Mechanical Engineering, National Chiao Tung University, Taiwan, ROC.*

****Associate Professor, Department of Electrical Engineering, Ta Hua University of Science and Technology, Taiwan, ROC.*

demonstrated the full mobility of six degrees of freedom that the five-axis machines however do not have. The slerp method for table-tilting-type five-axis machines is thus proposed in this paper to generate steady angular velocity of the interpolation curve. The simulation results are presented and compared with those produced using existing methods.

GEOMETRICAL ROTATION

Geometrical rotation is useful in the computer graphics domain, which involves displaying 3D models. The geometric interaction among objects, such as a workpiece cut by a milling tool demonstrated in real time, known as a cutting simulation, enables the CAM module or control designer to visualize the physics such as machine collision or undercutting and overcutting conditions. The vector motion is useful for demonstrating the position and orientation of a milling tool during cutting simulation. The key concern of motion planning in multi-axis CNC is how to attain constant-speed motion in the milling tool for higher machining quality. In recent years, a basic pipeline of CNC motion planning is that tool-path (position) planning is performed followed by tool-axis orientation planning. The tool-axis orientation planning modifies the tool-axis orientation of each cutter contact point to adhere to the speed and acceleration limits of each individual rotation axis. After the tool-tip position is determined through path planning by using techniques such as nonuniform rational basis spline to attain constant-speed interpolation in displacement, the rest of the milling tool body can be deviated from the tool-tip position due to the orientation. Orientation planning preferably yields a constant rotational speed.

2.1 Spherical linear interpolation of a unit vector motion

Unit vector motion occurs when one end of a unit is pinned at the origin and the other end moves on the unit sphere (Fig. 1). When the unit vector moves from point $\boldsymbol{p}_1$ to point $\boldsymbol{p}_2$, the two points $\boldsymbol{p}_1$ and $\boldsymbol{p}_2$ can be used to form the arc of a great circle on the unit sphere. The normal vector of this arc is derived from the cross product of the two position vectors $\boldsymbol{p}_1$ and $\boldsymbol{p}_2$ as follows:

$$\boldsymbol{n} = \boldsymbol{p}_1 \times \boldsymbol{p}_2 \tag{1}$$

The angle subtended by the arc may also be derived using

$$\Omega = arccos(\boldsymbol{p_1} \cdot \boldsymbol{p_2})$$

The position vector that lies on the great circle and is normal to $\boldsymbol{p}_1$ is then derived as follows.

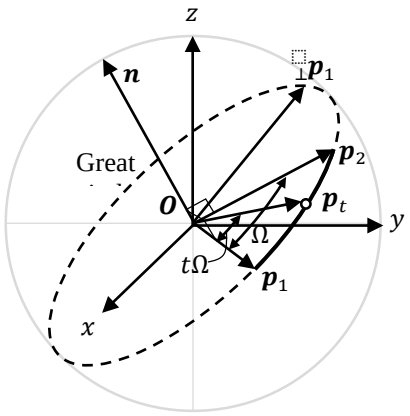

Fig. 1. Spherical linear interpolation of a unit vector.

$$_{\perp}\boldsymbol{p}_1 = \frac{\boldsymbol{n} \times \boldsymbol{p}_1}{|\boldsymbol{n} \times \boldsymbol{p}_1|} == \frac{\boldsymbol{p}_2 - \boldsymbol{p}_1 cos\Omega}{sin\Omega}$$

Let t be the parameter with $0 \le t \le 1$ and let $\boldsymbol{p}_t$ be the corresponding interpolation; Rodrigues' rotation formula yields the following:

$$\boldsymbol{p}_t = \boldsymbol{p}_1 \cos\theta + {}_{\perp}\boldsymbol{p}_1 \sin\theta + \boldsymbol{n}(\boldsymbol{n} \cdot \boldsymbol{p}_1)(1 - \cos\theta)$$

where $\theta = t\Omega$. Because $\boldsymbol{n} \cdot \boldsymbol{p}_1 = (\boldsymbol{p_1} \times \boldsymbol{p}_2) \cdot \boldsymbol{p}_1 = 0$,

$$\begin{aligned} \boldsymbol{p}_t &= \boldsymbol{p}_1 \cos(t\Omega) + {}_{\perp}\boldsymbol{p}_1 \sin(t\Omega) \\ &= \tfrac{\sin(\Omega - t\Omega)}{sin\Omega}\boldsymbol{p}_1 + \tfrac{\sin(t\Omega)}{sin\Omega}\boldsymbol{p}_2 \end{aligned} \tag{2}$$

The afore mentioned result is referred to as slerp, which refers to constant-speed motion along an arc of a great circle on which the vector ends on a unit sphere and the interpolation parameter t is between 0 and 1.

2.2 Axis–angle representation

The axis–angle representation of a rotation parameterizes it in a 3D Euclidean space on the basis of two quantities: a unit vector, $\boldsymbol{n}$, called the Euler axis, which indicates the direction of the axis of rotation, and an angle, θ, which describes the magnitude of the rotation around the axis, as shown in Fig. 2. Let $\boldsymbol{N}$ be the cross-product matrix, a skew-symmetric matrix, of $\boldsymbol{n}$ and

$$\boldsymbol{N} = \begin{bmatrix} 0 & -n_z & n_y \\ n_z & 0 & -n_x \\ -n_y & n_x & 0 \end{bmatrix}$$

$$\boldsymbol{N^2} = \begin{bmatrix} {n_x}^2 - 1 & n_x n_y & n_x n_z \\ n_x n_y & {n_y}^2 - 1 & n_y n_z \\ n_x n_z & n_y n_z & {n_z}^2 - 1 \end{bmatrix}$$

The rotational matrix based on a Lie algebra may be written as

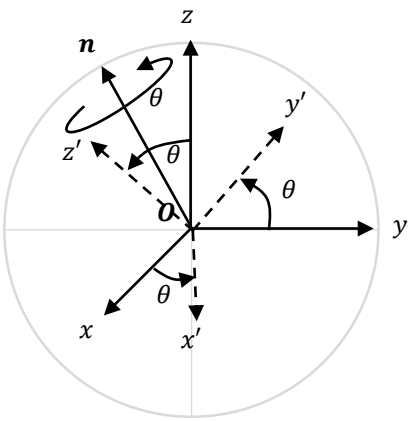

Fig. 2. Axis–angle representation.

$$\boldsymbol{R}(\boldsymbol{n},\theta) = e^{\theta \boldsymbol{N}} = \boldsymbol{I} + sin\theta \boldsymbol{N} + v\,\theta\,\boldsymbol{N}^2 \tag{3}$$

It is well known that

$$\boldsymbol{R}(\boldsymbol{n},-\boldsymbol{\theta})\boldsymbol{R}(\boldsymbol{n},\boldsymbol{\theta}) = \boldsymbol{e}^{\boldsymbol{\theta N}}\boldsymbol{e}^{-\boldsymbol{\theta N}} = \boldsymbol{e}^{\boldsymbol{\theta N}}/\boldsymbol{e}^{\boldsymbol{\theta N}} = \boldsymbol{I}$$

PHYSICAL ROTATION

Physical rotation is different from geometrical rotation because the mechanical structure, for example a gyroscope, robot, or five-axis machine, is physically integrated through bearings in a specific sequence. In other words, unlike geometrical rotation, physical rotation is dependent on the sequence of rotations. The axle bearings are highly accurate because a small amount of clearance or misalignment deliberately introduced to the system can cause either substantial friction or a large positioning error. In the assembly process, which must take account of the electrical wiring, and actuator weights are the key factors for the configuration of axle sequence. The rotary table, typically referred to as the C axis, is often mounted on top of a cradle-like structure, typically referred to as the A or B axis. Thus, the cradle-like structure must exert a larger torque than the rotary table during machining. The A and B axis use a larger servo motor and can be assembled to the five-axis machine earlier than the rotary table. To represent the physical meaning of machine assembly, Euler angles with three angles are used to describe the orientation of a rigid body with respect to a fixed coordinate system. They can represent the orientation of a mobile frame of reference in physics.

Euler angle transformation

Any orientation can be achieved by modifying three elemental rotations (that is, rotations about the axes of a coordinate system). Euler angles can be defined by three of these rotations. They can also be defined through elemental geometry, and the geometrical definition indicates that three rotations are always sufficient to reach any frame. There exist 12 possible sequences of rotation axes: ZXZ, XYX, YZY, ZYZ, XZX, YZY, XYZ, YZX, ZXY, XZY, ZYX, and YXZ. Extrinsic rotations are elemental rotations that occur about the axes of the fixed coordinate system. Intrinsic rotations are elemental rotations that occur about the axes of a coordinate system attached to a moving body. Among them, intrinsic rotations are commonly used in CNC machinery because of the simplicity of the mechanism's design. For example, the ZYX Euler angle transformation that maps the machine coordinate (fixed frame) to the workpiece coordinate (mobile frame) with the axis rotation sequence θ_A about the X axis, θ_B about the Y axis, and θ_C about the Z axis, as shown in Fig. 3, may be expressed as follows, where $c\,\theta = cos\,\theta$ and $s\,\theta = sin\,\theta$.

$$\boldsymbol{R}(\boldsymbol{z},\theta_C)\boldsymbol{R}(\boldsymbol{y},\theta_B)\boldsymbol{R}(\boldsymbol{x},\theta_A) = \begin{bmatrix} c\theta_C c\theta_B & c\theta_C s\theta_B s\theta_A - s\theta_C c\theta_A & c\theta_C s\theta_B c\theta_A + s\theta_C s\theta_A \\ s\theta_C c\theta_B & s\theta_C s\theta_B s\theta_A + c\theta_C c\theta_A & s\theta_C s\theta_B c\theta_A - c\theta_C s\theta_A \\ -s\theta_B & s\theta_A c\theta_B & c\theta_A c\theta_B \end{bmatrix} \tag{4}$$

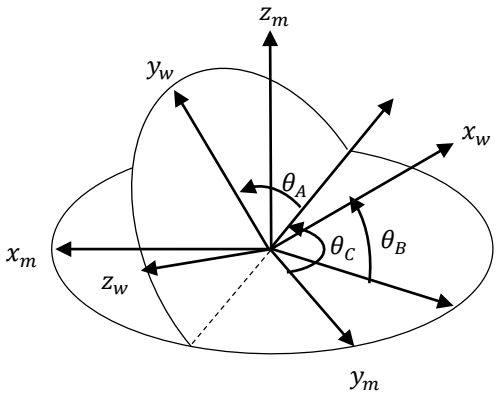

Fig. 3. Intrinsic ZYX transformation.

Setting $\theta_B = 0$ in the ZYX Euler angle transformation, a rotation identical to the ZXZ Euler angle transformation with the axis rotation sequence Z, X, Z when setting the first rotation around the Z axis in the sequence to zero can be obtained.

$$\boldsymbol{M}(\theta_A,\theta_C) = \boldsymbol{R}(\mathbf{z},\theta_C)\boldsymbol{R}(\boldsymbol{y},0)\boldsymbol{R}(\boldsymbol{x},\theta_A) = \begin{bmatrix} cos\theta_C & -sin\theta_C cos\theta_A & sin\theta_C sin\theta_A \\ sin\theta_C & cos\theta_C cos\theta_A & -cos\theta_C sin\theta_A \\ 0 & sin\theta_A & cos\theta_A \end{bmatrix} \tag{5}$$

The following inverse transformation is obtained:

$$\boldsymbol{M}^{-1}(\theta_A,\theta_C) = \boldsymbol{R}(\boldsymbol{x},-\theta_A)\boldsymbol{R}(\mathbf{z},-\theta_C)$$

The conversion between the Euler angle transformation to the axis–angle transformation may be achieved by simply comparing the matrix $\boldsymbol{M}(\theta_A, \theta_C)$ in (5) and the matrix $\boldsymbol{R}(\boldsymbol{n}, \theta)$ in (3) (Henderson, 1997).

$$n_x = sin\frac{\theta_A}{2}cos\frac{\theta_c}{2}/sin\phi$$
$$n_y = sin\frac{\theta_A}{2}sin\frac{\theta_c}{2}/sin\phi$$
$$n_z = cos\frac{\theta_A}{2}sin\frac{\theta_c}{2}L/sin\phi \quad (6)$$

where ϕ is half of the magnitude of the rotation θ in the axis–angle transformation and

$$\phi = \frac{\theta}{2} = arccos(cos\frac{\theta_A}{2}cos\frac{\theta_C}{2}). \quad (7)$$

Although there is no rotation about the Y axis in the ZYX Euler angle transformation (i.e., $\theta_B = 0$), the y component of the unit vector $\boldsymbol{n}$ (i.e., n_y) is nonzero when $sin\theta_A \neq 0$ and $sin\theta_C \neq 0$. By substituting the axis–angle transformation parameters in (6) and (7) back into (3), the transformation matrix identical to (5) can be obtained with $\theta_B = 0$ even when $n_y \neq 0$.
In the same manner as in the geometrical rotation, this physical rotation represented by the Euler angle transformation may be parameterized by three angles, but such parameterization is degenerated at some points on the hypersphere, leading to a problem concerning the gimbal lock that is discussed in Section 3.2.

Coordinate transformation in five-axis CNC machines

CNC can transform the cutter's location and orientation with respect to the workpiece coordinate system into axes positioned using the machine coordinate system. Lin *et al.* (2014) proposed several types of inverse kinematic transformation. Without loss of generality, a common type of five-axis CNC machine of a table-tilting type (i.e., an XYZAC type) is used as an example in this paper as shown in Fig. 4,

$$\begin{bmatrix} x_m \\ y_m \\ z_m \end{bmatrix} = \boldsymbol{M}^{-1}(\theta_A, \theta_C)\begin{bmatrix} x_w \\ y_w \\ z_w \end{bmatrix} + \boldsymbol{d}$$

where $\begin{bmatrix} x_m \\ y_m \\ z_m \end{bmatrix}$ is the machine coordinate and $\begin{bmatrix} x_w \\ y_w \\ z_w \end{bmatrix}$ is the workpiece coordinate. The XYZ linear translation induced by the guideway motion of the machine is stored in $\boldsymbol{d}$ and the rotation induced by rotary table motion is stored in θ_A and θ_C respectively. Although the axis of a milling tool is fixed to the spindle axis $\boldsymbol{S}$ in the machine coordinate, when viewed from the workpiece, it is rotated because of the rotary table motion.

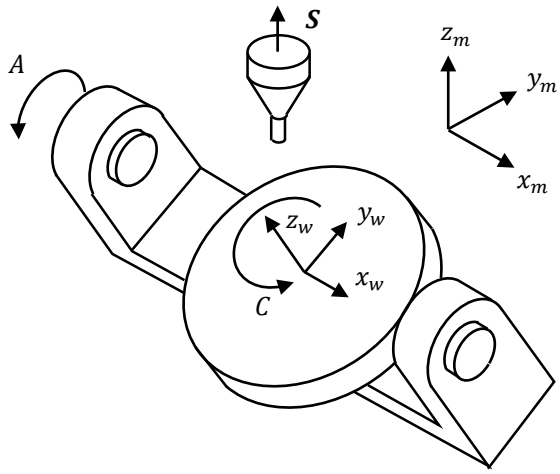

Fig. 4. Five-axis CNC machine of the XYZAC type (table-tilting machine).

$$\begin{bmatrix} x_{w,tool} \\ y_{w,tool} \\ z_{w,tool} \end{bmatrix} = \boldsymbol{M}(\theta_A, \theta_C)\boldsymbol{S}$$

The axis of a milling tool is typically in parallel with the Z axis (i.e., $\boldsymbol{S} = [0\ 0\ 1]^T$). The procedures for interpolating the tool axis may be as follows.

1) According to the cutter location data from the G-code command in the NC program, calculate the tool axis in the workpiece coordinate as follows:

$$^w\boldsymbol{p}_1 = \boldsymbol{M}(\theta_{A,1}, \theta_{C,1})\boldsymbol{S}$$
$$^w\boldsymbol{p}_2 = \boldsymbol{M}(\theta_{A,2}, \theta_{C,2})\boldsymbol{S}$$

2) According to the geometrical rotation, perform slerp from $^w\boldsymbol{p}_1$ and $^w\boldsymbol{p}_2$ to obtain $^w\boldsymbol{p}_t$ according to (2).
3) According to the physical model, identify $\theta_{A,t}$ and $\theta_{C,t}$ by solving

$$^w\boldsymbol{p}_t = \begin{bmatrix} \boldsymbol{x}_{w,tool,t} \\ \boldsymbol{y}_{w,tool,t} \\ \boldsymbol{z}_{w,tool,t} \end{bmatrix} = \boldsymbol{M}(\theta_{A,t}, \theta_{C,t})\boldsymbol{S}$$
$$= \begin{bmatrix} sin\theta_{C,t}sin\theta_{A,t} \\ -cos\theta_{C,t}sin\theta_{A,t} \\ cos\theta_{A,t} \end{bmatrix}. \quad (8)$$

The solution of (8) includes

$$\theta_{A,t} = \pm arccos(z_{w,tool,t}) \quad (9)$$
$$\theta_{C,t} = arctan(\frac{x_{w,tool,t}/sin\theta_{A,t}}{-y_{w,tool,t}/sin\theta_{A,t}}) \quad (10)$$

The solution of (9) suffers because $\theta_{A,t}$ may be either

positive or negative and must be checked against the results of neighboring solutions. One possible method is by predicting $\theta_{A,t}$ on the basis of the interpolation between $\theta_{A,1}$ and $\theta_{A,2}$ as follows.

$$\tilde{\theta}_{A,t} = \theta_{A,1}(1-t) + \theta_{A,2} \tag{11}$$

The resolution becomes

$$\theta_{A,t} = sign(\tilde{\theta}_{A,t})\, arccos(z_{w,tool,t})$$

where $sign(\tilde{\theta}_{A,t}) = -1$ when $\tilde{\theta}_{A,t} < 0$ and $sign(\tilde{\theta}_{A,t}) = 1$ otherwise. This formula causes unexpected discontinuity because the true solution of $\theta_{A,t}$ may be nonlinear with respect to t. The second problem occurs when $\boldsymbol{z}_{w,tool,t} = 1$ because it results in $sin\theta_{A,t} = 0$ and $\theta_{C,t}$ becomes indeterminate from (10). This phenomenon is also known as the gimbal lock.

The interpolation on the axis–angle transformation of a coordinate is different from the spherical linear interpolation of a pure unit vector because the coordinate frame has three orthogonal vectors. When the milling tool is treated as a coordinate frame such as

$$^{m}\boldsymbol{T} = [\,_{\perp}\boldsymbol{S} \times \boldsymbol{S}, \quad _{\perp}\boldsymbol{S}, \quad \boldsymbol{S}]$$

the angles θ_A and θ_C can be determined by solving the following equation without solving the gimbal-lock problem:

$$\boldsymbol{M}(\theta_A, \theta_C) = {}^{w}\boldsymbol{T}\,{}^{m}\boldsymbol{T}^{-1}$$

where

$$^{w}\boldsymbol{T} = [\,^{w}_{\perp}\boldsymbol{S} \times {}^{w}\boldsymbol{S}, \quad {}^{w}_{\perp}\boldsymbol{S}, \quad {}^{w}\boldsymbol{S}]$$

Quaternion slerp

The rotation quaternion when the coordinate frame rotation is taken into account may be applicable to the tool-axis-orientation planning in multi-axis CNC machining because it is unaffected by the gimbal-lock problem. When used to represent a rotation relative to a reference coordinate system, unit quaternions are called orientation quaternions or attitude quaternions. The axis–angle transformation can be represented by a rotation quaternion using an extension of Euler's formula:

$$\begin{aligned}\boldsymbol{q} &= q_0 + q_1\mathbf{i} + q_2\mathbf{j} + q_3\mathbf{k} = e^{\frac{\theta}{2}\boldsymbol{n}} \\ &= cos\frac{\theta}{2} + \boldsymbol{v}\, sin\frac{\theta}{2}\end{aligned} \tag{12}$$

where $\boldsymbol{v} = \tilde{\boldsymbol{n}} = n_x\mathbf{i} + n_y\mathbf{j} + n_z\mathbf{k}$, $\boldsymbol{n} = \begin{bmatrix} n_x \\ n_y \\ n_z \end{bmatrix}$ is the Euler axis, and θ is the magnitude of the rotation about the axis. Notably, $\mathbf{ii} = \mathbf{jj} = \mathbf{kk} = \mathbf{ijk} = -1$. Additionally,

$$\boldsymbol{q}^t = (e^{\frac{\theta}{2}\boldsymbol{n}})^t = e^{\frac{t\theta}{2}\boldsymbol{n}} = cos\frac{t\theta}{2} + \boldsymbol{v}\, sin\frac{t\theta}{2}$$

To perform two rotation quaternions of axis–angle transformation, a rotation of θ_A is first applied about the X axis followed by another rotation of θ_C about the Z axis:

$$\begin{aligned}{}^{A}_{0}\boldsymbol{q} &= \boldsymbol{e}^{\frac{\theta_A}{2}\boldsymbol{x}} = cos\tfrac{\theta_A}{2} + \boldsymbol{v}_x\, sin\tfrac{\theta_A}{2},\ \boldsymbol{v}_x = 1\mathbf{i} + 0\mathbf{j} + 0\mathbf{k} \\ {}^{C}_{A}\boldsymbol{q} &= \boldsymbol{e}^{\frac{\theta_C}{2}\boldsymbol{z}} = cos\tfrac{\theta_C}{2} + \boldsymbol{v}_z\, sin\tfrac{\theta_C}{2},\ \boldsymbol{v}_z = 0\mathbf{i} + 0\mathbf{j} + 1\mathbf{k}\end{aligned}$$

The two quaternions can be combined into one equivalent quaternion.

$$\begin{aligned}{}^{C}_{0}\boldsymbol{q} = {}^{C}_{A}\boldsymbol{q}\,{}^{A}_{\boldsymbol{0}}\boldsymbol{q} = {} & (cos\frac{\theta_C}{2} + \boldsymbol{v}_z\, sin\frac{\theta_C}{2})(cos\frac{\theta_A}{2} \\ & + \boldsymbol{v}_x\, sin\frac{\theta_A}{2}) \\ = {} & cos\frac{\theta_A}{2}cos\frac{\theta_C}{2} + sin\frac{\theta_A}{2}cos\frac{\theta_C}{2}\mathbf{i} \\ & + sin\tfrac{\theta_A}{2}sin\tfrac{\theta_C}{2}\mathbf{j} + cos\tfrac{\theta_A}{2}sin\tfrac{\theta_C}{2}\mathbf{k}\end{aligned} \tag{13}$$

In addition, ${}^{C}_{A}\boldsymbol{q}\,{}^{A}_{\boldsymbol{0}}\boldsymbol{q} \neq {}^{A}_{\boldsymbol{0}}\boldsymbol{q}\,{}^{C}_{A}\boldsymbol{q}$ holds because $\boldsymbol{z} \times \boldsymbol{x} \neq \boldsymbol{x} \times \boldsymbol{z}$; thus, the rotation quaternion can be used to distinguish different physical configurations or assembly sequences. The quaternion in (13) and the axis–angle transformation in (6) and (7) are consistent in the expression of the rotation quaternion. The quaternion combination is vital for controlling the rotational axis, which maps the workpiece coordinate into the machine coordinate system and vice versa. Two rotation quaternions,

$$\begin{aligned}{}^{1}_{0}\boldsymbol{q} &= \boldsymbol{e}^{\frac{\theta_1}{2}\boldsymbol{n_1}} = cos\frac{\theta_1}{2} + \boldsymbol{v}_1\, sin\frac{\theta_1}{2} \\ {}^{2}_{\boldsymbol{0}}\boldsymbol{q} &= \boldsymbol{e}^{\frac{\theta_2}{2}\boldsymbol{n_2}} = cos\frac{\theta_2}{2} + \boldsymbol{v}_2\, sin\frac{\theta_2}{2}\end{aligned}$$

can also be combined into one equivalent quaternion of relative rotation

$$\begin{aligned}{}^{2}_{1}\boldsymbol{q} &= {}^{2}_{0}\boldsymbol{q}({}^{1}_{0}\boldsymbol{q}^{-1}) \\ &= (cos\tfrac{\theta_1}{2}cos\tfrac{\theta_2}{2} + sin\tfrac{\theta_1}{2}sin\tfrac{\theta_2}{2}\boldsymbol{n}_2 \cdot \boldsymbol{n}_1) - \\ &sin\tfrac{\theta_1}{2}cos\tfrac{\theta_2}{2}\boldsymbol{v}_1 + \\ &\ sin\frac{\theta_1}{2}sin\frac{\theta_2}{2}\boldsymbol{v}_2 - cos\frac{\theta_1}{2}sin\frac{\theta_2}{2}\widetilde{\boldsymbol{n_2} \times \boldsymbol{n_1}}\end{aligned}$$

When slerp is applied to unit quaternions, the quaternion path maps a path through 3D rotations in a

standard manner. The effect is a rotation with uniform angular velocity around a fixed rotation axis. Let t be the parameter, $0 \le t \le 1$,

$$\boldsymbol{q}_t = ({}^2_1\boldsymbol{q})^t\,{}^1_0\boldsymbol{q} \;=\; ({}^1_2\boldsymbol{q})^{1-t}\,{}^2_0\boldsymbol{q} \tag{14}$$

It may also be treated as a four-dimensional vector and holds the slerp relationship. As shown in Fig. 5,

$$\boldsymbol{q}_t = \frac{sin(\Omega - t\Omega)}{sin\Omega}\,{}^1_0\boldsymbol{q} + \frac{sin(t\Omega)}{sin\Omega}\,{}^2_0\boldsymbol{q} \tag{15}$$

The angle subtended by the great arc of the four-dimensional space may also be derived by

$$\Omega = arccos(\boldsymbol{q}_1 \cdot \boldsymbol{q}_2)$$

It can be proven that (14) and (15) are equivalent statements (Dam, 1998), that is

$$({}^2_1\boldsymbol{q})^t\,{}^1_0\boldsymbol{q} = \frac{sin(\Omega - t\Omega)}{sin\Omega}\,{}^1_0\boldsymbol{q} + \frac{sin(t\Omega)}{sin\Omega}\,{}^2_0\boldsymbol{q} \tag{16}$$

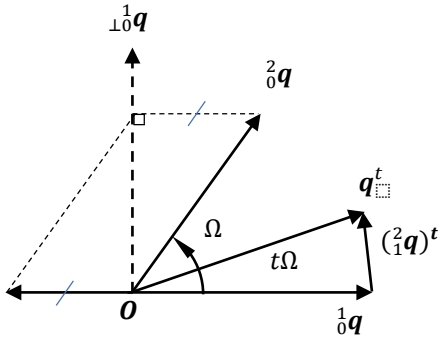

Fig. 5. General quaternion slerp.

The angular sweeping velocity in (14) and (15) was been shown to be constant when t increases with constant speed from 0 to 1. This constant rotational speed is vital for tool-orientation planning in the CNC machine when all Euler angles can be fulfilled by the physical structure of the machine. The result in (16) is also useful in tool-axis-orientation planning of a five-axis CNC machine of the XYZAC type because ${}^2_1\boldsymbol{q}$ can be derived from a relative rotation in the axis–angle transformation as follows:

$$\boldsymbol{R}(\boldsymbol{n}, \theta) = \boldsymbol{M}(\theta_{A,2}, \theta_{C,2})\boldsymbol{M}^{-1}(\theta_{A,1}, \theta_{C,1})$$

However, whether the quaternion remains in the AC plane when both the starting and end rotations lie on the AC plane is unclear. The following demonstration explains why it does not remain in the AC plane.

$$\boldsymbol{M}(\theta_{A,2}, \theta_{C,2})\boldsymbol{M}^{-1}(\theta_{A,1}, \theta_{C,1})$$

$$= \begin{bmatrix} m_{11} & m_{12} & m_{13} \\ m_{21} & m_{22} & m_{23} \\ m_{31} & m_{32} & m_{33} \end{bmatrix} \tag{17}$$

The entry $m_{31} = sin\theta_{A,2}sin\theta_{C,1}$ is nonzero when $sin\theta_{A,2} \neq 0$ and $sin\theta_{C,1} \neq 0$. Comparing (17) with (6) indicates that B rotation (i.e., rotation around the Y axis) is required. However this is not required by $({}^2_1\boldsymbol{q})^t$ when $t \neq 0$ for a five-axis CNC machine of the XYZAC type. That is, to achieve quaternion slerp stated in (15), a six-axis XYZABC machine is needed. Six-axis machines are suitable for many robotics applications but not to five-axis CNC machines of any type, including the rotation tool center point (RTCP) type.

Five-axis slerp

Five-axis slerp improved from quaternion slerp is proposed to yield superior axis-tool-orientation planning. It is identical to quaternion slerp in the gimbal-lock locations, for example, when $\theta_A = 0$ in five-axis CNC machines of the XYZAC type. The rest of the tool-axis-orientation planning is derived from tool-axis slerp provided that only one of the axes is obtained from quaternion slerp. Taking the five-axis CNC machine of the XYZAC type as an example, the quaternion obtained from (15) can be converted into

$$\boldsymbol{q_t} = q_{t,0} + q_{t,1}\mathbf{i} + q_{t,2}\mathbf{j} + q_{t,3}\mathbf{k}$$

where

$$q_{t,i} = a(t)\,{}^1_0q_i + b(t){}^2_0q_i,\; i = 1, 2, 3 \tag{18}$$

and

$$a(t) = \frac{sin(\Omega - t\Omega)}{sin\Omega},\quad b(t) = \frac{sin(t\Omega)}{sin\Omega}$$

to the axis–angle transformation by comparing (12) and (3).

$$\boldsymbol{M} = \begin{bmatrix} 1 - 2(q_{t,3}^2 + q_{t,4}^2) & 2(q_{t,2}q_{t,3} - q_1q_4) & 2(q_{t,2}q_{t,4} + q_{t,1}q_{t,3}) \\ 2(q_{t,2}q_3 + q_{t,1}q_{t,4}) & 1 - 2(q_{t,2}^2 + q_{t,4}^2) & 2(q_{t,3}q_{t,4} - q_{t,1}q_{t,2}) \\ 2(q_{t,2}q_{t,4} - q_{t,1}q_{t,3}) & 2(q_{t,3}q_{t,4} + q_{t,1}q_{t,2}) & 1 - 2(q_{t,2}^2 + q_{t,3}^2) \end{bmatrix} \tag{19}$$

Then, $\theta_{A,q,t}$ is obtained from $\boldsymbol{M}$ of the quaternion and the ZYX Euler angle transformation in (4) as follows:

$$\theta_{A,q,t} = arctan\left(\frac{2(q_{t,3}q_{t,4} + q_{t,1}q_{t,2})}{1 - 2(q_{t,2}^2 + q_{t,3}^2)}\right) \tag{20}$$

Equation (20) is valid for $-\pi \le \theta_{A,q,t} \le \pi$ when $|\theta_{B,t}| < 90^0$, which is true in quaternion slerp when $\theta_{B,0} = \theta_{B,1} = 0^0$. Finally, $\theta_{C,t}$ is solved by assuming

that $\theta_{B,t} = 0$ in the ZYX Euler angle transformation. As shown in (4),

$$\theta_{C,t} = arctan\left(\frac{(q_{t,2}q_{t,4}+q_{t,1}q_{t,3})/sin\theta_{A,q,t}}{(q_{t,3}q_{t,4}-q_{t,1}q_{t,2})/sin\theta_{A,q,t}}\right) \quad (21)$$

This result is replaced by the quaternion slerp result in the gimbal-lock position $\theta_{A,t} = 0$. In the vicinity of the gimbal-lock position, $\theta_{C,t}$ is identical to the rotation quaternion for the ZYX Euler angle transformation in which

$$\theta_{C,t} = \theta_{C,q,t} = arctan\left(\frac{2(q_{t,3}q_{t,4}+q_{t,1}q_{t,2})}{1-2(q_{t,2}^2+q_{t,3}^2)}\right) \quad (22)$$

The gimbal lock is not a problem for quaternion slerp because the entry $m_{31} = sin\theta_{A,2}sin\theta_{C,1}$ of $\boldsymbol{M}$ is zero when $sin\theta_{A,2} = 0$ or $sin\theta_{C,1} = 0$. The vicinity of the gimbal lock region should be excluded by inserting a pair of G codes into the NC program at the positions where the tool-axis-orientation planning of quaternion slerp passes through the region of the gimbal lock as shown in Fig. 6.

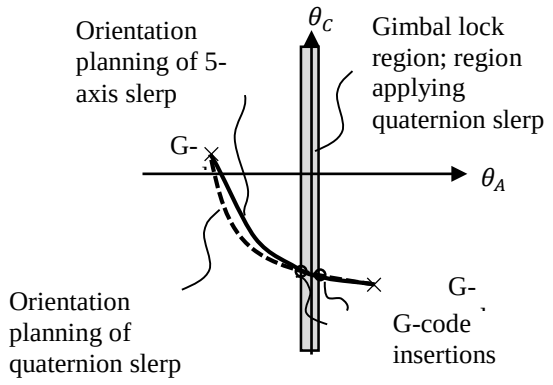

Fig. 6. Insertion of G codes into NC program.

RESULTS AND COMPARISONS

The methods introduced herein are listed and compared as follows.

1. Tool-axis slerp method: According to (20) to (22), perform tool-axis-orientation planning on the basis of the milling-tool-axis change of one block of G-code commands.
2. Quaternion slerp method: According to (20) to (22), perform tool-axis-orientation planning from the relative rotation transformation of one block of G-code commands.
3. Five-axis slerp method: According to (20) to (22), perform tool-axis-orientation planning from the relative rotation transformation of one block of G-code commands by inserting G codes into the gimbal lock region.

The results are obtained for an XYZAC machine with the following specifications:

A-axis swiveling range: 200° (100° to −100°)
C-axis rotation range: 360°

The maximum angle subtended by the great arc between two adjacent angular interpolations is set as 0.02°. The maximum rotational speed of all axes is set as 0.03°/command.

The NC program with six G-code command blocks is listed as follows for benchmarking.

N00 G00 A0.0 C0.0;	Block #0: Homing position
N01 G1 A-10.0 C-10.0;	Block #1: Test rotation starting behavior
N02 A-60.0 C60.0;	Block #2: Tool-orientation-planning results for short travel
N03 A-70.0 C220.0;	Block #3: Tool-orientation-planning results for large travel
N04 A40.0 C180.0;	Block #6: Test large-travel gimbal-lock-region behavior
N05 A40.0 C50.0;	Block #5: Large travel at positive A-axis position.
N06 A0.0 C0.0;	Block #6: Test rotation ending behavior
N07 A40.0 C50.0;	The following blocks mirror the previous ones for verification.
N08 A40.0 C180.0;	
N09 A-70.0 C220.0;	
N10 A-60.0 C60.0;	
N11 G1 A-10.0 C-10.0;	
N12 A0.0 C0.0;	

The results from the compared slerp methods are shown in Fig. 7. None of the methods exhibited hysteresis; in other words, they provided the same result when the starting and end points of each command block were interchanged. In five-axis CNC machine tools, the milling tool typically scans the contour offset or zig-zag on the projection plane and uses the surfaces of the reference model to determine the tool orientation for the workpiece to be machined. When the zig-zag scan is applied, many back-and-forth NC command blocks occur on a similar trajectory on the workpiece surface. During the zig-zag scan, the hysteresis can impose different machining patterns on adjacent cutting paths and downgrade machining quality. All methods satisfy this similarity condition, at least on the AC plane. Fig. 7 shows that, from block 3 to block 4, a grave gimbal-lock problem hinders the tool-axis slerp method. The same gimbal-lock problem occurs on block 0 to block 1 and block 5 to block 6. Fig. 7 also reveals that the tool-axis slerp method

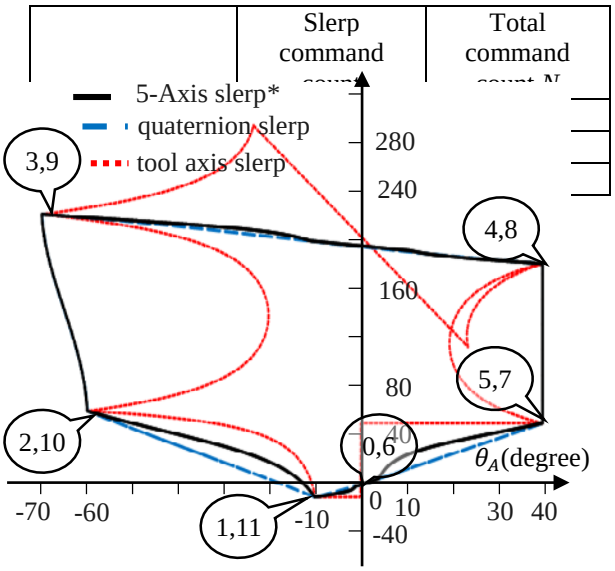

maintains the tool axis on the great arc in Cartesian space (the workpiece coordinate system) and tends to cause greater rotation variation than does quaternion slerp. This implies that quaternion slerp does follow the great arc in Cartesian space, which maintains the constant-speed of the machine coordinate system.

Fig. 7. Tool axis orientation planning in the AC plane.

In Fig. 8, the A-, B-, and C-axis rotations of quaternion slerp for six-axis machines, such as robots, are shown in terms of the command count *n* divided by the total number of commands *N*, which are shown and compared for various methods in Table I. The required rotation of the B axis, which is absent in the five-axis XYZAC-type CNC machine, is nonzero, and the maximum value of $\theta_{B,t}$ is approximately 15°. The effect of nonzero B rotation is shared by the rotation of the AC axes for five-axis slerp.

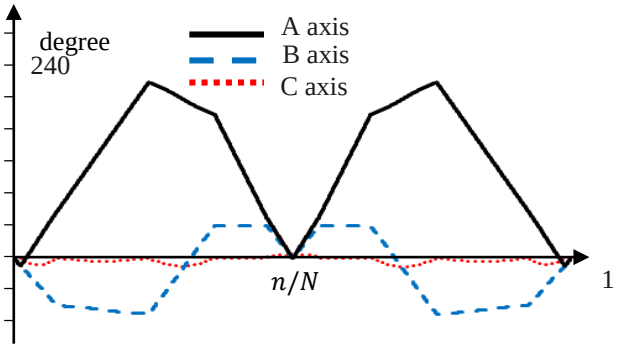

Fig. 8. A-, B-, and C-axis rotations for six-axis machines

Table 1. The command counts of tool orientation planning.

Fig. 9 reveals that the gimbal-lock position induces θ_A discontinuity in the vicinity of $\theta_A = 0$ when the tool-axis method is used. In Fig. 10, C-axis (or Z-axis) rotation is shown in terms of the command count *n* divided by the total number of commands *N*. The gimbal-lock problem can induce solution branching on C-axis rotation when the tool-axis method is used.

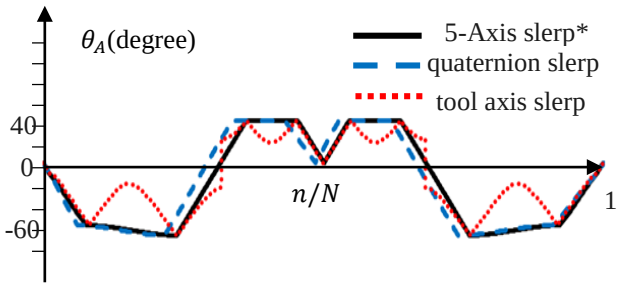

Fig. 9. A-axis rotation on the planning path.

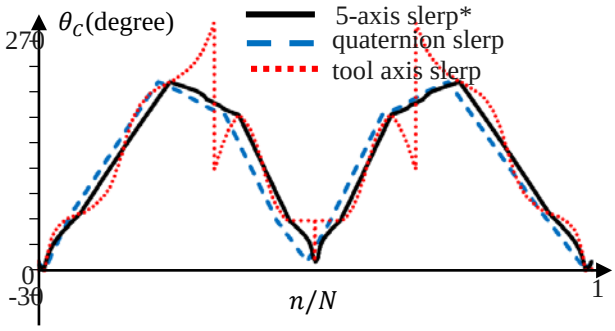

Fig. 10. C-axis rotation on planning path.

The enlarged C-axis-rotation plot shown in Fig. 11 indicates that the motion of quaternion slerp is faster than the other method when it commences, which explains why phase shifts occur between quaternion slerp and five-axis slerp in both Fig. 10 and 11. However, because the total number of commands *N* for both quaternion slerp and five-axis slerp are similar, angular motion deceleration must occur in quaternion slerp during the ending period. This phenomenon can be observed in Fig. 12. The angle subtended by the great arc between the two adjacent angular

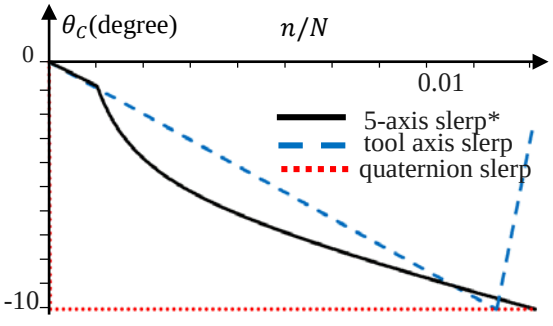

Fig. 11. C-axis rotation starting behavior

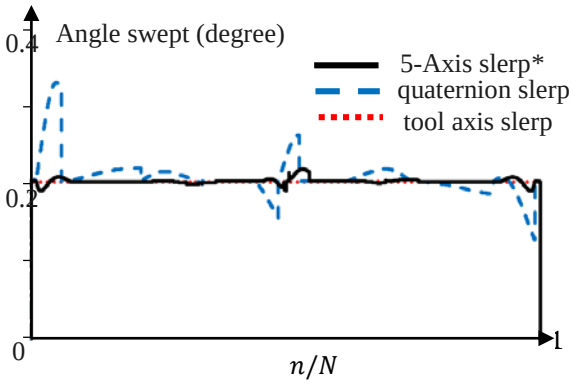

Fig. 12. Angle subtended by the great arc between two adjacent angular interpolations.

interpolations remains constant in tool-axis slerp.different machining patterns on adjacent cutting paths and lowers machining quality. Five-axis slerp yields a maximum angle variation of 8% that is acceptable for most high-precision applications because of the CAM software that generates G codes and because NC programs generally subdivide the NC commands into 0.1°–1° increments, which considerably reduces angle variation; moreover, the angle variation is symmetrical on the start and end commands.

Table 2 compares slerp methods; the five-axis slerp method is viable for all criteria. Fig. 13 demonstrates the notebook deburring process by using a five-axis XYZAC-type machine. Under such conditions, nonconstant tool-axis-orientation planning of the quaternion slerp method can cause overcutting or undercutting situation as shown in Fig. 13(c). Fig. 14 demonstrates the gimbal-lock problem, which may occur when the tool-axis slerp method is used when the C axis approaches 0°. Although Fig. 14 illustrates a five-axis RTCP-type machine, the same gimbal-lock problem can occur in five-axis XYZAC-type CNC machines.

Table 2. Comparisons between different slerp methods

	Total command count (machining time)	Constant speed of rotation (machining quality)	Gimbal-lock problem (control stability)
five-axis slerp	Good	Good	Good
quaternion slerp	Best	Bad	Best
tool-axis slerp	Bad	Best	Bad

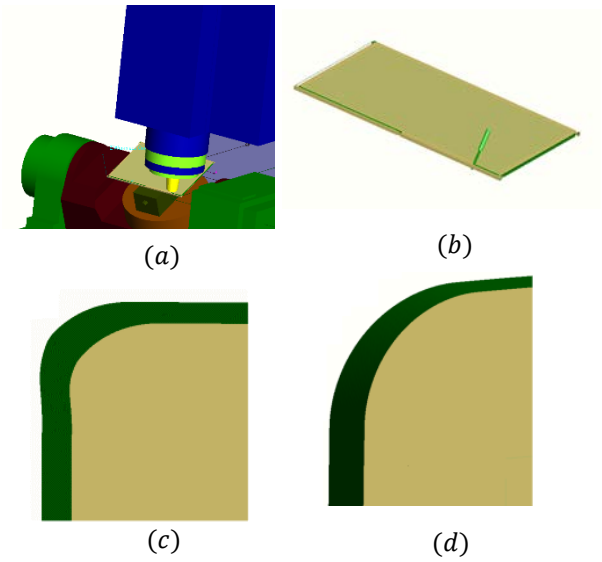

Fig. 13. Simulation of a five-axis XYZAC-type machine: (a) machine view, (b) workpiece view, (c) corner machined through nonconstant-speed tool-axis-orientation planning by using the quaternion slerp method, and (d) corner machined through constant-speed tool-axis-orientation planning by using five-axis slerp method.

CONCLUSION

This paper explains the failure of quaternion slerp when it is employed to attain constant rotational-speed motion. This paper demonstrates that the gimbal-lock problem occurs when the tool-axis slerp method is used. Tool-axis slerp requires more machining time because of the discontinuity and rotational-speed limit. This study developed an innovative method of tool-axis-orientation planning, called five-axis slerp, to achieve nearly constant rotational-speed motion. Although this paper demonstrated the result only on a specific five-axis CNC machine of the XYZAC type, the method is suitable for five-axis CNC machines with three translation and two rotation axes of any type.

ACKNOWLEDGMENT

The authors thank Dept. of Industry Technology of Ministry of Economic Affairs, R.O.C. for financially supporting this research under Project No. 107-EC-17-A-05-S4-006.

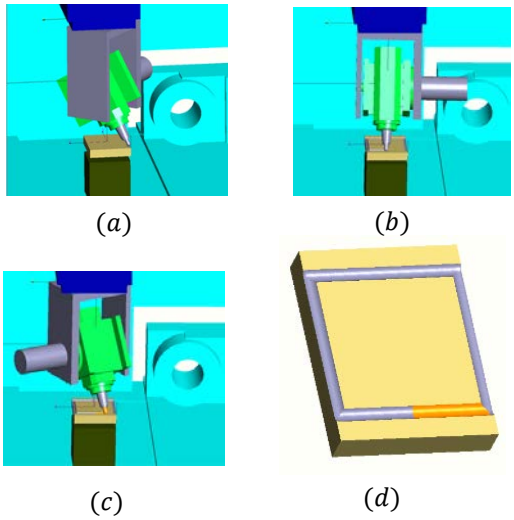

Fig. 14. Simulation of a five-axis RTCP-type machine with the tool-axis slerp method (a) when cutting starts, (b) in the vicinity of the gimbal-lock position, (c) and when the C axis rotates 180° at the gimbal-lock position. (d) Final product indicates the discontinuity of machining.

REFERENCES

Barr, A. H., Currin, B., Gabriel, S., and Hughes, J. F., "Smooth Interpolation of Orientations with Angular Velocity Constraints using Quaternions", *Computer Graphics*, Vol. 26, No. 2, pp. 313-320, (1992).

Dam, E. B., Koch, M., and Lillholm, M., "Quaternions, Interpolation and Animation", *Technical Report*, Department of Computer Science, University of Copenhagen (1998).

Henderson, D. M., "Euler Angles, Quaternions, and Transformation Matrices – Working Relationships", *Technical Report*, NASA (1977).

Ho, M.-C., Hwang, Y.-R., and Hu, C.-H., "Five-Axis Tool Orientation Smoothing Using Quaternion Interpolation Algorithm", *International Journal of Machine Tools and Manufacture*, Vol. 43, No. 12, pp. 1259-1267 (2003).

Li, P. and Guo, R., "Research on Quaternion-Quintic Spherical Bezier Spline Interpolation Algorithm for 5-Axis Machining", *Proceedings of 4th International Conference on Computer Science and Education*, pp. 612-617 (2009).

Lin, A.C., Lin, T.K., and Lin, T.D., "Deriving Generic Transformation Matrices for Multi-Axis Milling Machine", *International Journal of Mechanical and Mechatronics Engineering*, Vol. 8, No. 7, pp. 1231-1235 (2014).

Ramamoorthi, R. and Barr, A. H., "Fast Construction of Accurate Quaternion Splines", *SIGGRAPH '97 Proceedings of the 24th Annual Conference on Computer Graphics and Interactive Techniques*, pp. 287-292, (1997).

Shoemake, K., "Animating rotation with quaternion curves", *Computer Graphics*, Vol. 19, No. 3, pp. 245-254 (1985).

Zhang, K. and Zhang, L., "Five-Axis Machining Cutter Axis Vector Optimization Based on Quaternions", *International Journal of Engineering and Technical Research*, Vol. 2, No. 8, pp. 67-69 (2014).

Zhao, X., Zhao, H., Li, X., and Ding, H., "Path Smoothing for Five-Axis Machine Tools Using Dual Quaternion Approximation with Dominant Points", *International Journal of Precision Engineering and Manufacturing*, Vol. 18, No. 5, pp. 711-720 (2017).

五軸球面線性插值用於五軸數控機中刀具定向規劃

嚴昌道 成維華
國立交通大學 機械工程系

鄭時龍
大華科技大學 電機工程系

摘 要

一般數值控制的四元數球面線性插值方法（slerp）不適用於五軸數控機機中的刀具軸定向規劃。本文解釋了為什麼四元數slerp方法無法實現恆定轉速。當四元數slerp方法用於五軸加工時，加工品質會降低。 為了彌補這一缺失，本文提出了一種工具軸定向規劃的解決方案，即五軸slerp方法，它可以應用於插值曲線的穩定角速度。